ACS OMEGA

Article

Cite This: ACS Omega 2018, 3, 3036−3044

Impact of Electrical Conductivity on the Electrochemical Performances of Layered Structure Lithium Trivanadate ($LiV_{3-x}M_xO_8$, M= Zn/Co/Fe/Sn/Ti/Zr/Nb/Mo, x = 0.01−0.1) as Cathode Materials for Energy Storage

P. Senthil Kumar,[†,‡,§] Sakunthala Ayyasamy,*[,‡] Eng Soon Tok,[†] Stefan Adams,[∥] and M. V. Reddy*[,†,§,∥]

[†]Department of Physics, National University of Singapore, 117 542, Singapore

[‡]Department of Physics, Karunya University, Coimbatore 641 114, Tamilnadu, India

[§]Department of Physics, KPR Institute of Engineering and Technology, Coimbatore 641 407, Tamilnadu, India

[∥]Department of Materials Science and Engineering, National University of Singapore, 117576, Singapore

Supporting Information

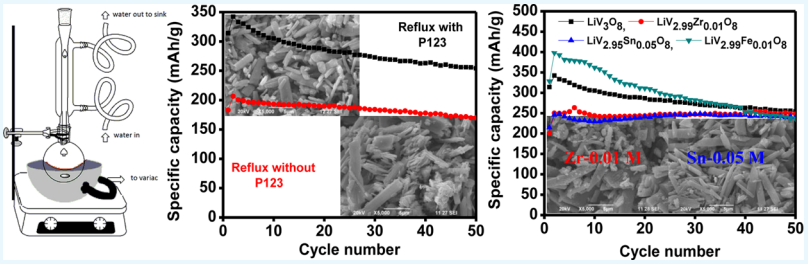

ABSTRACT: Pristine trivanadate (LiV_3O_8) and doped lithium trivanadate ($LiV_{3-x}M_xO_8$, M = Zn/Co/Fe/Sn/Ti/Zr/Nb/Mo, x = 0.01/0.05/0.1 M) compounds were prepared by a simple reflux method in the presence of the polymer, Pluronic P123, as the chelating agent. For comparison, pristine LiV_3O_8 alone was also prepared in the absence of the chelating agent. The Rietveld-refined X-ray diffraction patterns shows all compounds to exist in the layered monoclinic LiV_3O_8 phase belonging to the space group of $P2_1/m$. Scanning electron microscopy analysis shows the particles to exhibit layers of submicron-sized particles. The electrochemical performances of the coin cells were compared at a current density of 30 mA/g in the voltage window of 2−4 V. The cells made with compounds $LiV_{2.99}Zr_{0.01}O_8$ and $LiV_{2.95}Sn_{0.05}O_8$ show a high discharge capacity of 245 ± 5 mA h/g, with an excellent stability of 98% at the end of the 50th cycle. The second cycle discharge capacity of 398 mA h/g was obtained for the compound $LiV_{2.99}Fe_{0.01}O_8$, and its capacity retention was found to be 58% after 50 cycles. The electrochemical performances of the cells were correlated with the electrical properties and the changes in the structural parameters of the compounds.

INTRODUCTION

Secondary lithium ion batteries with high energy density, power density, and long cycling stability are considered as the heart of the growing mobile technology and future electric vehicles. For intensive commercial applications, drawbacks such as costly battery materials and the safety issues associated with them have to be addressed. Layered structured cathode materials such as lithium trivanadate (LiV_3O_8), vanadium pentoxide (V_2O_5), and other vanadium derivatives have good scope for lithium ion battery technology because of their low cost, high energy density, and better safety features.[1−5] LiV_3O_8 (LVO) is a nonlithiated cathode material in which the lithium ions can freely intercalate into and deintercalate from the LVO's layered structure, exhibiting better structural stability than V_2O_5 and other vanadium derivatives.[6−9] It has a layered monoclinic structure with a space group of $P2_1/m$, reported by Wadsley in 1957.[10] It consists of V−O layers arranged one above the other made up of two interconnected units by corner-sharing oxygen atoms, such as the VO_6 octahedra unit and VO_5 trigonal bipyramid units, providing structural stability.[11−13]

However, practical batteries with LVO electrodes show capacity degradation and poor rate performance because of their low electrical conductivity.[14] This was significantly overcome by means of cation doping such as Na, K, Cu, and Ag in the lithium site and Mo, Si, Mn, Ni, Cr, and so forth in the vanadium sites.[15−22] But the clear role of doping on the electrical property of the compound LiV_3O_8 and its influence on the electrochemical performance of the cell have not been reported in any of the literature. Research on the inter-relation between the oxidation states of metal ions, the role of ionic and electronic conductivities of the compound, and the electrochemical performance of the battery is the need of the hour for the betterment of battery materials. Recently, our group

Received: December 1, 2017
Accepted: February 26, 2018
Published: March 13, 2018

DOI: 10.1021/acsomega.7b01904
ACS Omega 2018, 3, 3036−3044

reported on the correlation between the electrical and electrochemical performance of the cathode materials, $LiNi_{0.5}Mn_{0.5}O_2$ and $LiNi_{1/3}Co_{1/3}Mn_{1/3}O_2$.[23,24] In the present work, lithium trivanadate and $LiV_{3-x}M_xO_8$ (M = Zn/Co/Fe/Sn/Ti/Zr/Nb/Mo) compounds with dopants of different oxidation states were prepared at different levels of doping x = 0.01/0.05/0.1 M. The changes in the electrical properties of the compound upon doping were explored. The materials were prepared by a very simple and cost-effective Pluronic P123-assisted reflux method. Studies on the doping effect of Zn/Fe/Sn/Nb at the vanadium site of LiV_3O_8 have not been reported elsewhere.

RESULTS AND DISCUSSION

Structure and Morphology. X-ray diffraction (XRD) patterns of LVO-P, LVO-WP, and doped compounds (0.05 M level of doping) are shown in Figure 1a,b (Figure S1a,b for 0.01

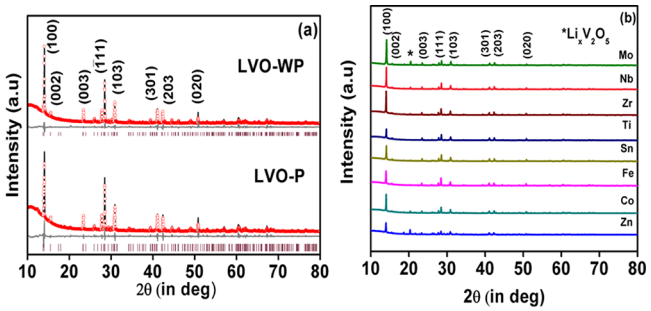

Figure 1. (a) Rietveld-refined XRD patterns of LVO-P and LVO-WP. (b) XRD pattern of $LiV_{2.95}M_{0.05}O_8$ (M = Zn/Co/Fe/Sn/Ti/Zr/Nb/Mo) compounds.

and 0.1 M level doped compounds, respectively). The XRD patterns of all compounds correspond to the layered monoclinic crystalline phase with space group $P2_1/m$.[13−15] The lattice parameter values for LVO-P and LVO-WP were found to be a = 6.700 Å, b = 3.625 Å, and c = 12.096 Å and a = 6.619 Å, b = 3.578 Å, and c = 11.939 Å, respectively. The lattice parameters "a", "b," and "c" were found to be in the range of 6.516−6.772, 3.485−3.677, and 11.835−12.241 Å, respectively, for doped compounds and are given in Table 1. The lattice parameter values of all compounds were found closely matched with JCPDS card no. 72-1193.

On comparison with LVO-P, the shift in the peak corresponding to the (100) plane either toward the higher or lower 2θ angle (Figure 2) and significant changes in the intensity of the (100) plane was observed for all doped compounds. Shifting of the peak corresponding to the (100) plane toward lower 2θ angle indicates the increase in the interlayer distance d_{100} and vice versa (Table S1). The increase in d_{100} could be better for the Li^+ ion insertion and reinsertion, which will lead to better electrochemical performance. On comparison with LVO-P, the shift in the peak corresponding to the (100) plane toward the lower 2θ value was observed for the compounds $LiV_{2.99}Zr_{0.01}O_8$, $LiV_{2.95}Sn_{0.05}O_8$, and $LiV_{2.99}Fe_{0.01}O_8$, as shown in Figure 2d. The interlayer distance value (d_{100}) was found to be 6.352, 6.356, 6.366, and 6.370 Å for the compounds LVO-P, $LiV_{2.99}Zr_{0.01}O_8$, $LiV_{2.95}Sn_{0.05}O_8$, and $LiV_{2.99}Fe_{0.01}O_8$, respectively. The XRD pattern of the compound $LiV_{2.9}Co_{0.1}O_8$ shows a very low interlayer distance value (d_{100} ≈ 5.951 Å), which may result in poor electrochemical performance. All compounds show minor peaks at 2θ ≈ 22°, corresponding to the $Li_xV_2O_5$ phase (5−10%), which is commonly observed in the LiV_3O_8 compound prepared through any of the reported methods,[25−30] and are considered as an active phase in LiV_3O_8, which helps in improving the electrochemical performance of the battery.[13] No other impurity phases were observed at any of the doping level.

Figure 3 shows the morphology of the selected compounds, LVO-P, LVO-WP, $LiV_{2.99}Zr_{0.01}O_8$, $LiV_{2.99}Fe_{0.01}O_8$, and

Table 1. Lattice Parameters from Rietveld-Refined XRD Patterns

doping level	compound	a (Å)	b (Å)	c (Å)
	LVO-P	6.700	3.625	12.096
	LVO-WP	6.619	3.578	11.939
0.01 M	$LiZn_{0.01}V_{2.99}O_8$	6.654	3.603	12.051
	$LiCo_{0.01}V_{2.99}O_8$	6.667	3.607	12.034
	$LiFe_{0.01}V_{2.99}O_8$	6.642	3.591	11.980
	$LiSn_{0.01}V_{2.99}O_8$	6.655	3.600	12.011
	$LiTi_{0.01}V_{2.99}O_8$	6.581	3.561	11.879
	$LiZr_{0.01}V_{2.99}O_8$	6.593	3.564	11.891
	$LiNb_{0.01}V_{2.99}O_8$	6.651	3.596	12.000
	$LiMo_{0.01}V_{2.99}O_8$	6.649	3.599	12.012
0.05 M	$LiZn_{0.05}V_{2.95}O_8$	6.597	3.563	11.878
	$LiCo_{0.05}V_{2.95}O_8$	6.663	3.603	12.016
	$LiFe_{0.05}V_{2.95}O_8$	6.571	3.550	11.835
	$LiSn_{0.05}V_{2.95}O_8$	6.576	3.554	11.852
	$LiTi_{0.05}V_{2.95}O_8$	6.583	3.559	11.872
	$LiZr_{0.05}V_{2.95}O_8$	6.603	3.567	11.886
	$LiNb_{0.05}V_{2.95}O_8$	6.664	3.605	12.024
	$LiMo_{0.05}V_{2.95}O_8$	6.607	3.581	11.944
0.1 M	$LiZn_{0.1}V_{2.9}O_8$	6.561	3.496	11.765
	$LiCo_{0.1}V_{2.9}O_8$	6.772	3.677	12.241
	$LiFe_{0.1}V_{2.9}O_8$	6.541	3.569	11.878
	$LiSn_{0.1}V_{2.9}O_8$	6.516	3.485	11.862
	$LiTi_{0.1}V_{2.9}O_8$	6.581	3.559	11.883
	$LiZr_{0.1}V_{2.9}O_8$	6.591	3.560	11.874
	$LiNb_{0.1}V_{2.9}O_8$	6.585	3.562	11.880
	$LiMo_{0.1}V_{2.9}O_8$	6.627	3.594	11.988

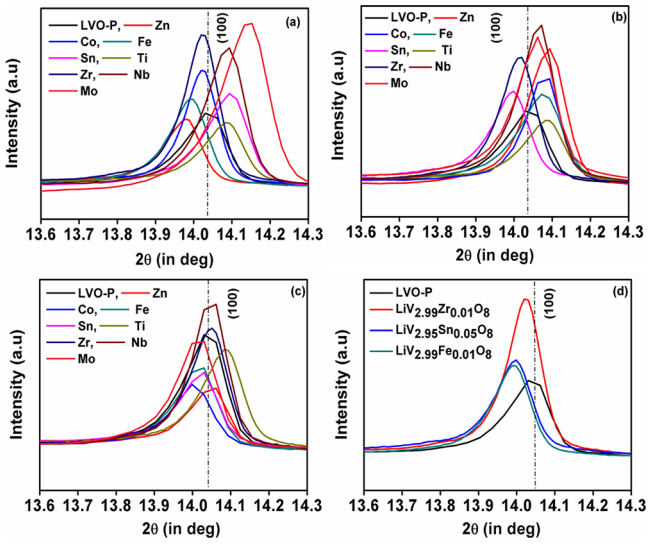

Figure 2. Peak shift corresponding to the (100) plane in (a) $LiV_{2.99}M_{0.01}O_8$, (b) $LiV_{2.95}M_{0.05}O_8$, (c) $LiV_{2.9}M_{0.1}O_8$ (M = Zn/Co/Fe/Sn/Ti/Zr/Nb/Mo) compounds, and (d) LVO-P, $LiV_{2.99}Zr_{0.01}O_8$, $LiV_{2.95}Sn_{0.05}O_8$, and $LiV_{2.99}Fe_{0.01}O_8$ compounds.

DOI: 10.1021/acsomega.7b01904
ACS Omega 2018, 3, 3036−3044

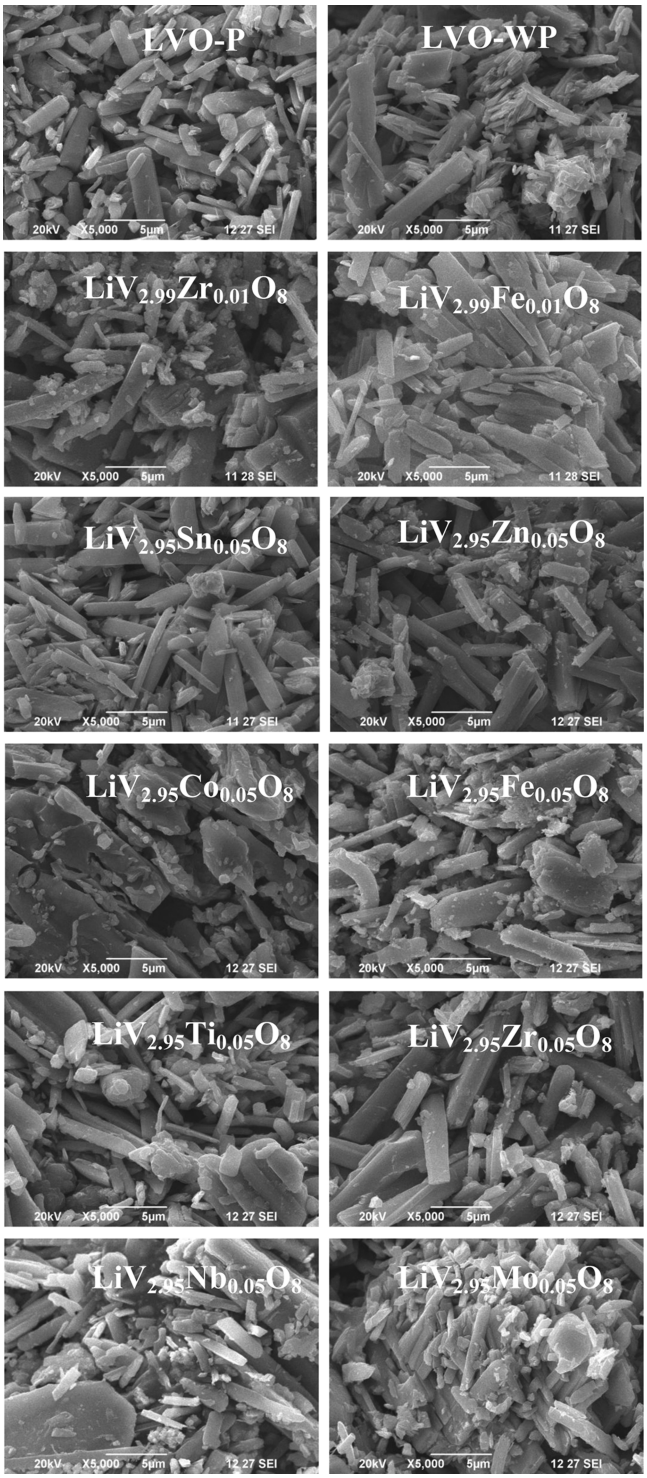

Figure 3. SEM images of bare and doped LiV_3O_8 compounds.

$LiV_{2.95}Sn_{0.05}O_8$, and other 0.05 M level doped compounds. Scanning electron microscopy (SEM) analysis shows the particles to have submicron-sized particles. Rod-shaped structures can be clearly observed for the compound LVO-P and Zn, Zr, Sn, Fe-doped compounds ranging in length from 4 to 10 μm. The irregular-shaped particles were observed for LVO-WP. Changes in particle sizes were observed upon doping. The BET surface area and pore volume were found to be 0.68, 0.57, 1.20, 1.11, and 1.01 m^2/g and 0.16, 0.13, 0.28, 0.26, and 0.23 cm^3/g for the compounds LVO-P, LVO-WP, $LiV_{2.99}Zr_{0.01}O_8$, $LiV_{2.99}Fe_{0.01}O_8$, and $LiV_{2.95}Sn_{0.05}O_8$, respectively. The morphologies of 0.01 and 0.1 M level of doped compounds were also found to have rod-shaped submicron-sized particles (images not shown).

Raman Spectroscopy and Electrical Studies. Raman and electrical studies were carried out for the parent and selected doped compounds based on their better electrochemical performance (to be discussed under galvanostatic studies).

Raman analysis is considered as a more suitable method to investigate the effect of dopants on the LiV_3O_8 crystal lattice. The Raman spectra of the select compounds are shown in Figure 4a,b. For LVO-P and LVO-WP, the observed band at

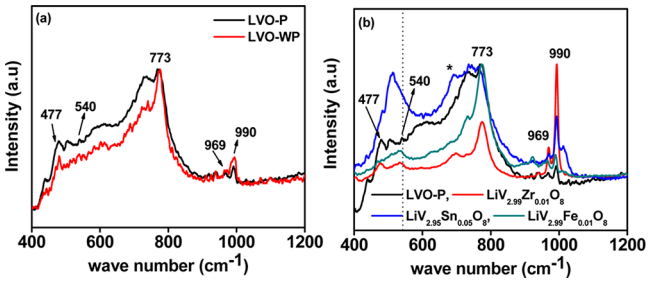

Figure 4. Raman spectra for (a) LVO-P and LVO-WP and (b) compounds LVO-P, $LiV_{2.99}Zr_{0.01}O_8$, $LiV_{2.99}Fe_{0.01}O_8$, and $LiV_{2.95}Sn_{0.05}O_8$.

773 cm^{-1} is related to the atomic motions of the corner-sharing oxygen among the VO_6, VO_5, and LiO_6 polyhedrons of LiV_3O_8.[31] The Raman bands at 990 and 969 cm^{-1} could be attributed to the V−O stretching vibrations of VO_5 pyramids. The weak vibrations of the B_{1g} and A_g symmetry species of LiV_3O_8 were observed at 540 and 477 cm^{-1}, respectively.[32]

The changes in the peak position and relative intensities between the peaks for doped compounds shown in Figure 4b indicate doping effect. The minor peak corresponding to the $Li_xV_2O_5$ phase was observed for all compounds (indicated by * symbol), as discussed earlier in the XRD section. The vibrations of the B_{1g} and A_g symmetry species were shifted to a lower wave number region in the order of $LiV_{2.95}Sn_{0.05}O_8$, $LiV_{2.95}Zr_{0.01}O_8$, and $LiV_{2.95}Fe_{0.01}O_8$. This indicated the rapid formation of VO_5 and VO_6 polyhedrons and thus a little distortion of the crystal lattice upon doping[32] because the ionic radii of doping ions are greater than that of V^{5+}. Moreover, the intensity ratio between the two peaks at 990 and 773 cm^{-1} were found to be in the order of $LiV_{2.99}Zr_{0.01}O_8$ > $LiV_{2.99}Fe_{0.01}O_8$ > $LiV_{2.95}Sn_{0.05}O_8$ > LVO-P compound. This behavior suggests that the formation rate of VO_5 and VO_6 polyhedrons of $V_3O_8^-$ layers was much faster than the superposition rate of $V_3O_8^-$ layers linked by the interlayered Li^+ ions in $LiV_{2.95}Zr_{0.01}O_8$.[31,32]

Electrical Studies. On the basis of the electrochemical performances (to be discussed later), electrical studies were conducted for the selected compounds LVO-P, LVO-WP, $LiZr_{0.01}V_{2.99}O_8$, $LiSn_{0.05}V_{2.95}O_8$, $LiFe_{0.01}V_{2.99}O_8$, and other doped $LiV_{2.95}M_{0.05}O_8$ (M = Zn/Co/Fe/Ti/Zr/Nb/Mo) compounds by means of ac impedance, four-probe method, and transference number studies.[23,24] Figure 5a represents the complex impedance plot for LVO-P, LVO-WP, $LiZr_{0.01}V_{2.99}O_8$, $LiSn_{0.05}V_{2.95}O_8$, and $LiFe_{0.01}V_{2.99}O_8$ taken at room temperature (303 K) in the frequency range of 42 Hz to 1 MHz. The Nyquist plot shows the overlapping of two semicircles related to the parallel combination of a resistor and a capacitor. High-

DOI: 10.1021/acsomega.7b01904
ACS Omega 2018, 3, 3036−3044

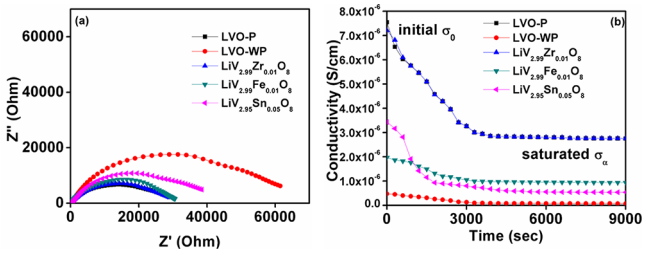

Figure 5. (a) Nyquist plot (Z' vs $-Z''$) and (b) transference number measurements for compounds LVO-P, LVO-WP, $LiV_{2.99}Zr_{0.01}O_8$, $LiV_{2.99}Fe_{0.01}O_8$, and $LiV_{2.95}Sn_{0.05}O_8$.

frequency semicircle is attributed to the grain, and low-frequency semicircle is related to the grain boundary effect.[23] The bulk resistance (R_b) of the sample was calculated by the intercept of the high-frequency semicircle on the x-axis. The electrical conductivity was calculated using the conductivity formula $\sigma = l/R_bA$, where "l" and "A" are the thickness and area of the pellet, respectively (Table 2) and the values were verified with the conductivity values calculated from the mid-frequency plateau region in the conductivity spectra (Figure S2). For comparison, the dc four-probe conductivity value was also measured from the V/I spectra (Figure S3) and matched with the impedance analysis. This validates our measurements. The compound LVO-P shows 1 order of higher electrical conductivity (10^{-6} S/cm) than the compound LVO-WP (10^{-7} S/cm). The electrical conductivity of doped compounds was in the order of $\sim 10^{-6}$ S/cm.

Simple and well-known wagner polarization method was used to find the ionic and electronic transference numbers (t_i and t_e) for all as-prepared compounds.[23,24] The change in current (I) was measured by applying a steady dc potential of 50 mV across the pellets. It was found that the initial conductivity values calculated from the observed current was decreasing with increasing time, before getting saturated. Significant differences were observed in the case of the percentage of ionic and electronic conduction, as calculated from the transference number measurements (Figure 5b) using the formula

$$t_i = \left(\frac{\sigma_o - \sigma_\alpha}{\sigma_o}\right) \quad (1)$$

where "σ_0" and "σ_α" are the initial and saturated conductivity values, respectively. The difference between the initial and saturated conductivity values gives the value of the ionic transference number.

Whereas the compound LVO-P showed 81% of ionic and 19% of electronic conductivity, the compound LVO-WP was found to have 74% of ionic and 26% of electronic conductivity. A very good mixed conductivity was observed in the case of compounds $LiV_{2.99}Zr_{0.01}O_8$ and $LiV_{2.95}Sn_{0.05}O_8$ with ~60% of ionic and ~40% of electronic conductivity. For all other doped compounds, $LiV_{2.95}M_{0.05}O_8$ (M = Zn, Co, Fe, Ti, Zr, Nb, and Mo), mixed conductivity was observed, as given in Table 2.

Electrochemical Analysis. *Cyclic Voltammetry (CV).* Cyclic voltammetry is one of the well adopted technique to understand redox potentials and complement the galvanostatic cycling profiles of cathode materials.[33−35] Figure 6a shows the

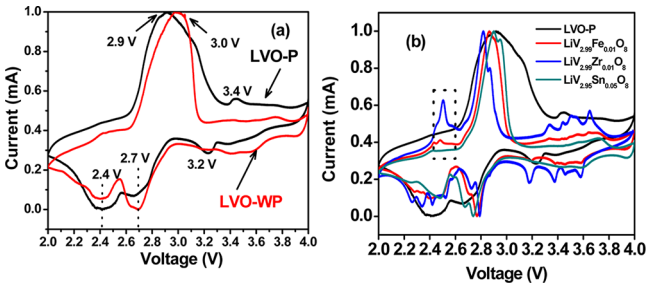

Figure 6. Comparative second cycle CV plots of cells made with (a) LVO-P and LVO-WP, (b) LVO-P, $LiV_{2.99}Zr_{0.01}O_8$, $LiV_{2.95}Sn_{0.05}O_8$, and $LiV_{2.99}Fe_{0.01}O_8$ (scan rate: 0.058 mV/s).

second cycle CV plots for the compounds LVO-P and LVO-WP. During intercalation, broad peaks were observed at 2.9 and 3.0 V for the compounds LVO-P and LVO-WP, respectively. The shift in the anodic peak toward the lower potential side in the case of LVO-P indicates the better kinetics for lithium deintercalation. Whereas the cathodic peak 2.7 V refers to single-phase reaction of lithium intercalation at tetrahedral sites, the peak at 2.4 V refers to lithium intercalation at octahedral sites resulting in two-phase transformation between $Li_3V_3O_8$ and $Li_4V_3O_8$.[36−38] The cathodic peak at 2.3 V expected due to the slow kinetic reaction as seen in many reports was not observed in the present work. This indicates the absence of any V^{3+} ion dissolution in the electrolyte. The cathodic peak at 2.6 V, usually observed due to the presence of $Li_{0.3}V_2O_5$, was not

Table 2. Data from Electrical Studies of the As-Prepared Compounds

	conductivity (S/cm) (±0.1)			transference number (±0.02)	
samples	Nyquist plot	conductivity spectra	dc four-probe	ionic (t_i)	electronic (t_e)
LVO-P	7.93×10^{-6}	8.12×10^{-6}	7.59×10^{-6}	**0.81**	**0.19**
LVO-WP	6.49×10^{-7}	6.58×10^{-7}	6.67×10^{-7}	0.77	0.23
$LiV_{2.99}Zr_{0.01}O_8$	7.28×10^{-6}	7.14×10^{-6}	6.97×10^{-6}	**0.60**	**0.40**
$LiV_{2.99}Fe_{0.01}O_8$	5.16×10^{-6}	5.14×10^{-6}	5.59×10^{-6}	**0.83**	**0.17**
$LiV_{2.95}Sn_{0.05}O_8$	6.68×10^{-6}	6.54×10^{-6}	6.49×10^{-6}	**0.61**	**0.39**
$LiV_{2.95}Zn_{0.05}O_8$	4.98×10^{-6}	5.17×10^{-6}	5.03×10^{-6}	0.76	0.24
$LiV_{2.95}Co_{0.05}O_8$	2.98×10^{-6}	3.11×10^{-6}	2.91×10^{-6}	0.74	0.26
$LiV_{2.95}Fe_{0.05}O_8$	4.76×10^{-6}	4.91×10^{-6}	5.04×10^{-6}	0.75	0.25
$LiV_{2.95}Ti_{0.05}O_8$	4.67×10^{-6}	4.74×10^{-6}	4.83×10^{-6}	0.78	0.22
$LiV_{2.95}Zr_{0.05}O_8$	5.27×10^{-6}	5.34×10^{-6}	5.47×10^{-6}	0.79	0.21
$LiV_{2.95}Nb_{0.05}O_8$	4.35×10^{-6}	4.44×10^{-6}	4.39×10^{-6}	0.76	0.24
$LiV_{2.95}Mo_{0.05}O_8$	4.68×10^{-6}	4.74×10^{-6}	4.85×10^{-6}	0.69	0.31

DOI: 10.1021/acsomega.7b01904
ACS Omega 2018, 3, 3036−3044

observed for both the compounds.[13] The anodic/cathodic peak around 3.4/3.2 V observed in the case of LVO-P shows a trace of $Li_{0.3}V_2O_5$ because of different energy sites for lithium ions.

In Figure 6b, the comparison of the second cycle CV plots (for compounds selected based on their high specific-discharge capacity and better cycling stability, to be discussed in the galvanostatic charge−discharge section) shows that the anodic peaks were shifted to lower potentials in the order of LVO-P, $LiV_{2.95}Sn_{0.05}O_8$, $LiV_{2.99}Fe_{0.01}O_8$, and $LiV_{2.99}Zr_{0.01}O_8$. The cathodic peaks were found to shift to higher potentials in the same order as mentioned above. This indicates the compound $LiV_{2.99}Zr_{0.01}O_8$ to have better lithium diffusion kinetics. The CV of compound $LiV_{2.99}Zr_{0.01}O_8$ shows an anodic peak around 2.5 V, which indicates easy accessibility of lithium sites during deintercalation.[39] As seen in Figure 7a, the anodic peak at 2.5 V was suppressed in the case of 0.05 and 0.1 M level of zirconium doping. Irrespective of dopants, a similar trend was observed for all compounds (Figure 7a−h). This indicates the accessibility of lithium ion sites to be affected by the level of doping. The anodic and cathodic peaks around ∼3.6 V in the case of all doped samples show deintercalation and intercalation of lithium ions, respectively, in the octahedral lithium site of the LiV_3O_8 host structure.[36−38]

In the case of $LiV_{3-x}Zr_xO_8$ compounds, the anodic and cathodic peaks were shifted to lower and higher potential sides, respectively, in the case of 0.01 and 0.05 M levels of doping, when compared to 0.1 M level of doping (Figure 7a). This indicates that doping more than 0.05 M of zirconium at the vanadium site results in poor lithium diffusion kinetics. The cathodic peaks at ∼3.2 and 3.4 V were observed in the CV plot of $LiV_{2.99}Zr_{0.01}O_8$ (indicated by arrow marks in Figure 8a), but not seen in the case of other two levels of doping. The above peaks were due to the presence of the $Li_{0.3}V_2O_5$ phase, holding different energy sites for lithium ions,[40−42] as discussed in XRD (indicated by * symbol in Figure 1b). Similar cathodic peaks belonging to the $Li_{0.3}V_2O_5$ phase were also observed in the case of other doped samples, depending on the type of doping and doping level (Figure 7b−h). For $LiV_{3-x}Sn_xO_8$ compounds (Figure 7b) and in the case of other doped samples as in Figure 8, expected anodic/cathodic peaks were observed, indicating good lithium diffusion at all levels of doping.

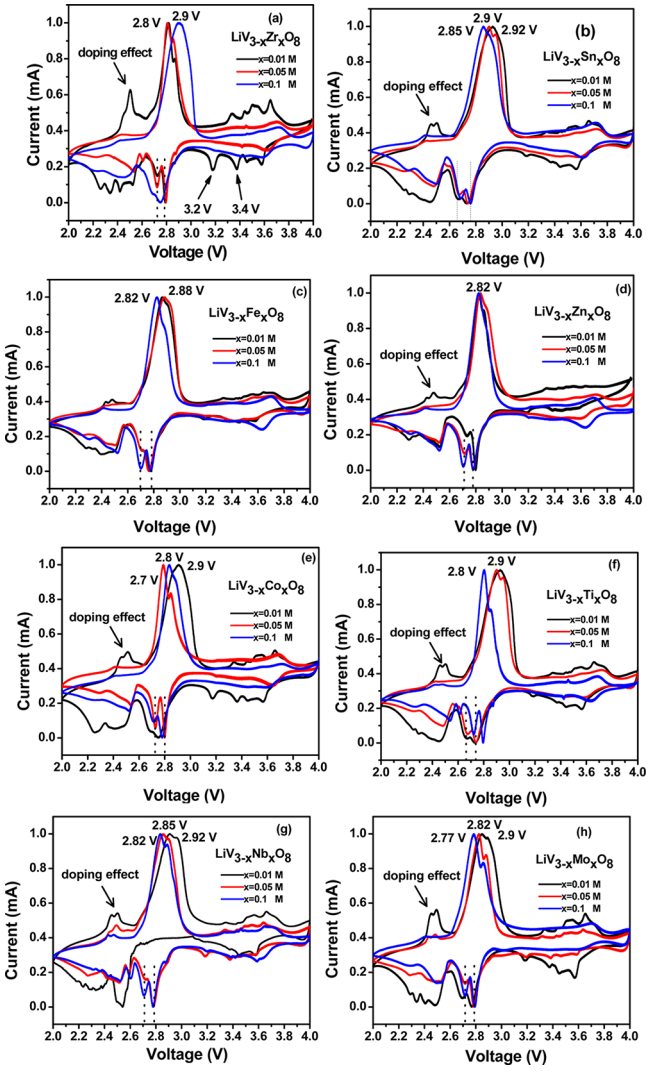

Figure 7. Second cycle CV plots of cells made with (a) $LiV_{3-x}Zr_xO_8$, (b) $LiV_{3-x}Sn_xO_8$, (c) $LiV_{3-x}Fe_xO_8$, (d) $LiV_{3-x}Zn_xO_8$, (e) $LiV_{3-x}Co_xO_8$, (f) $LiV_{3-x}Ti_xO_8$, (g) $LiV_{3-x}Nb_xO_8$, and (h) $LiV_{3-x}Mo_xO_8$ (x = 0.01/0.05/0.1 M); scan rate: 0.058 mV/s.

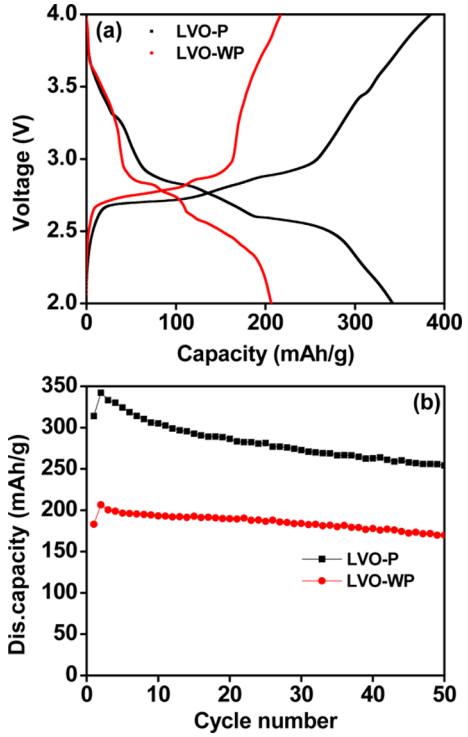

Figure 8. (a) Second cycle charge−discharge profiles and (b) cycling stability for LVO-P and LVO-WP.

Charge−Discharge Studies. Figure 8a shows the second cycle charge−discharge curves of cells made with LVO-P and LVO-WP. During the discharge, a clear two-step intercalation process was observed. In the case of LVO-P, the plateau regions around 2.7 and 2.4 V during the discharge refer to the lithium intercalation at tetrahedral and octahedral sites, respectively, of the LiV_3O_8 structure and were in accordance with the cathodic peaks observed in CV.[36−39] Cycling stability could be observed in Figure 8b. The 2nd and 50th cycle discharge capacity values are given in Table 3. The compound LVO-P was found to deliver the highest discharge capacity of 342 mA h/g at the 2nd cycle with a capacity retention of 71% at the end of the 50th

DOI: 10.1021/acsomega.7b01904
ACS Omega 2018, 3, 3036−3044

Table 3. Discharge Capacity of All Compounds

doping level	compound	discharge capacity (mA h/g) (±3 mA h/g) 2nd cycle	50th cycle	capacity retention at 50th cycle	irreversible capacity loss
	LVO-P	**342**	**254**	**71**	41
	LVO-WP	206	169	82	12
0.01 M	$LiV_{2.99}Zn_{0.01}O_8$	343	234	60	54
	$LiV_{2.99}Co_{0.01}O_8$	303	238	78	47
	$LiV_{2.99}Fe_{0.01}O_8$	**398**	**236**	**59**	78
	$LiV_{2.99}Sn_{0.01}O_8$	289	251	86	10
	$LiV_{2.99}Ti_{0.01}O_8$	325	196	60	51
	$LiV_{2.99}Zr_{0.01}O_8$	**250**	**247**	**98**	25
	$LiV_{2.99}Nb_{0.01}O_8$	340	234	68	18
	$LiV_{2.99}Mo_{0.01}O_8$	292	205	70	18
0.05 M	$LiV_{2.95}Zn_{0.05}O_8$	239	225	94	5
	$LiV_{2.95}Co_{0.05}O_8$	154	150	97	8
	$LiV_{2.95}Fe_{0.05}O_8$	211	206	97	7
	$LiV_{2.95}Sn_{0.05}O_8$	**245**	**241**	**98**	9
	$LiV_{2.95}Ti_{0.05}O_8$	225	211	93	15
	$LiV_{2.95}Zr_{0.05}O_8$	242	190	75	23
	$LiV_{2.95}Nb_{0.05}O_8$	192	164	85	3
	$LiV_{2.95}Mo_{0.05}O_8$	202	187	92	4
0.1 M	$LiV_{2.9}Zn_{0.1}O_8$	201	185	91	3
	$LiV_{2.9}Co_{0.1}O_8$	113	91	81	12
	$LiV_{2.9}Fe_{0.1}O_8$	196	160	82	6
	$LiV_{2.9}Sn_{0.1}O_8$	210	174	82	10
	$LiV_{2.9}Ti_{0.1}O_8$	172	162	94	25
	$LiV_{2.9}Zr_{0.1}O_8$	189	179	94	5
	$LiV_{2.9}Nb_{0.1}O_8$	192	120	62	2
	$LiV_{2.9}Mo_{0.1}O_8$	203	135	66	3

cycle, whereas the compound LVO-WP delivered a comparatively low discharge capacity of 206 mA h/g at the 2nd cycle and showed a capacity retention of 82% at the end of the 50th cycle.

The second cycle charge−discharge curves for 0.01, 0.05, and 0.1 M level doped LiV_3O_8 compounds are shown in Figure 9a−c. The second cycle discharge capacity values are given in Table 3. For the doped compounds, irrespective of the dopants, a high capacity was observed in the case of 0.01 M level of doping. This was in accordance with the CV plots, showing broader peaks for 0.01 M level of doping, as discussed above. The highest discharge capacity of 398 mA h/g was observed in the case of the $LiFe_{0.01}V_{2.99}O_8$ compound at the end of the second cycle, which was the highest discharge capacity among all compounds. When compared to LVO-P, a close value of the second cycle discharge capacity was observed for the compounds $LiV_{2.99}Zn_{0.01}O_8$, and $LiV_{2.99}Nb_{0.01}O_8$. Among doped compounds, very low second cycle discharge capacity was observed for compounds $LiV_{2.95}Co_{0.05}O_8$ and $LiV_{2.9}Co_{0.1}O_8$.

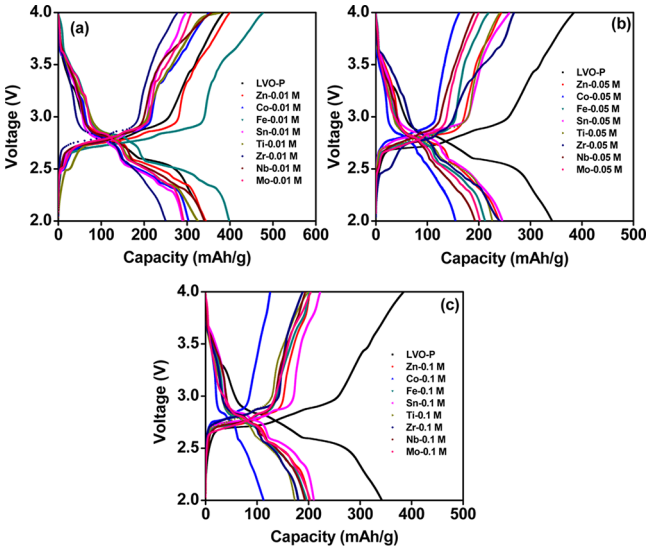

Figure 9. Second cycle charge−discharge profiles of (a) LVO-P and $LiV_{2.99}M_{0.01}O_8$, (b) LVO-P and $LiV_{2.95}M_{0.05}O_8$, and (c) LVO-P and $LiV_{2.9}M_{0.1}O_8$ (M = Zn/Co/Fe/Sn/Ti/Zr/Nb/Mo) compounds.

Cycling Stability of Doped Compounds. As seen in Figure 10a−h, better cycling stability was observed for $LiV_{3-x}M_xO_8$ (M = Zn, Co, Fe, Sn, Ti, Zr, Nb, and Mo) compounds with x = 0.05 M level of doping. Only in the case of zirconium, 0.01 M level of doping was found to be better than 0.05 and 0.1 M doped compounds, in terms of cycling stability. Among the zirconium-doped compounds, $LiV_{2.99}Zr_{0.01}O_8$ delivers a dis-

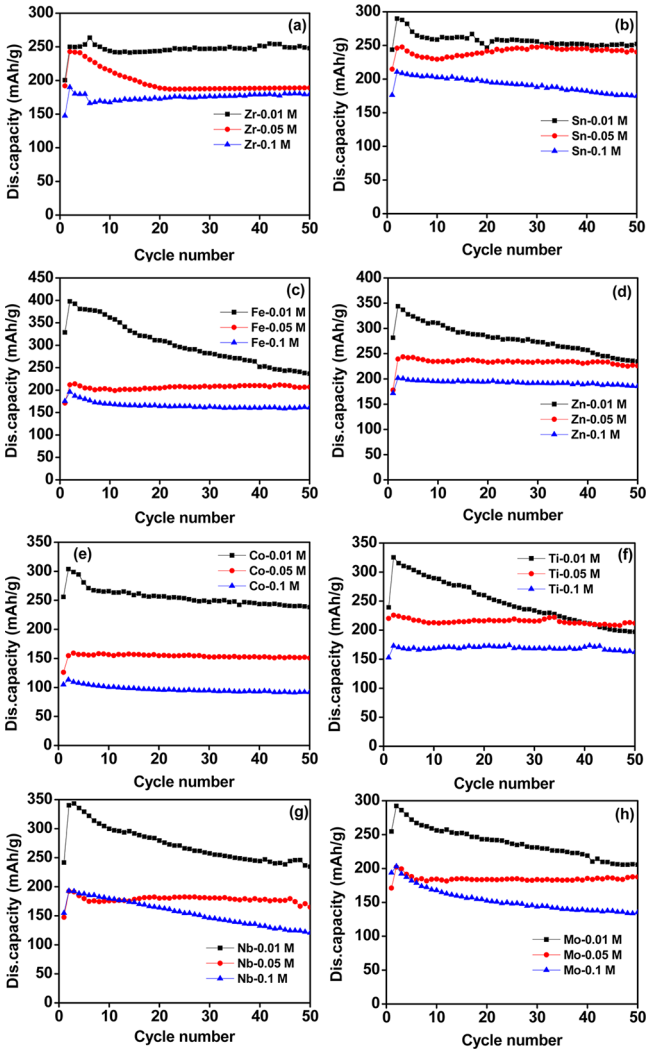

Figure 10. Cycling stability of cells made with (a) $LiV_{3-x}Zr_xO_8$, (b) $LiV_{3-x}Sn_xO_8$, (c) $LiV_{3-x}Fe_xO_8$, (d) $LiV_{3-x}Zn_xO_8$ (e) $LiV_{3-x}Co_xO_8$ (f) $LiV_{3-x}Ti_xO_8$, (g) $LiV_{3-x}Nb_xO_8$, and (h) $LiV_{3-x}Mo_xO_8$ (x = 0.01/0.05/0.1 M).

DOI: 10.1021/acsomega.7b01904
ACS Omega 2018, 3, 3036−3044

charge capacity of 250 and 247 mA h/g at the end of the 2nd and 50th cycles, respectively, with an excellent capacity retention of 98%, whereas further doping of zirconium degraded the electrochemical performance. Ren et al.[9] reported on $LiV_{3-x}Zr_xO_8$ (x = 0.00, 0.02, 0.04, 0.06, and 0.08) prepared by the citrate sol−gel method, and concluded the x = 0.06 M level of doping to be the best. They reported a discharge capacity of 269 and 246 mA h/g at the end of the 2nd and 50th cycles, respectively, for 0.1 C rate at the voltage window of 1.8−4.0 V. This indicates a stability of 92%. The present work shows the best capacity and stability for 0.1 C rate at the 0.01 M level of doping and is degraded for higher level of doping. This indicates that the preparation method chosen plays a key role in determining the optimized doping level to get the best electrochemical performance of the cells. Among the tin-doped compounds, $LiV_{2.95}Sn_{0.05}O_8$ delivers a discharge capacity of 245 and 241 mA h/g at the end of the 2nd and 50th cycles, respectively, with an excellent capacity retention of 98%. For $LiV_{2.99}Sn_{0.01}O_8$, although the cycling stability was only 86%, still it shows a better discharge capacity of 251 mA h/g at the 50th cycle. However, the performance was degraded in the case of high level of doping $LiV_{2.9}Sn_{0.1}O_8$. Therefore, the compounds, $LiV_{2.99}Zr_{0.01}O_8$, and $LiV_{2.95}Sn_{0.05}O_8$, could be concluded as the best in terms of capacity and stability among the doped compounds. The comparative cycling stabilities of the compounds $LiV_{2.99}Zr_{0.01}O_8$, $LiV_{2.95}Sn_{0.05}O_8$, LVO-P, and $LiV_{2.99}$ $Fe_{0.01}O_8$ are shown in Figure 11. Song et al.,[39] reported

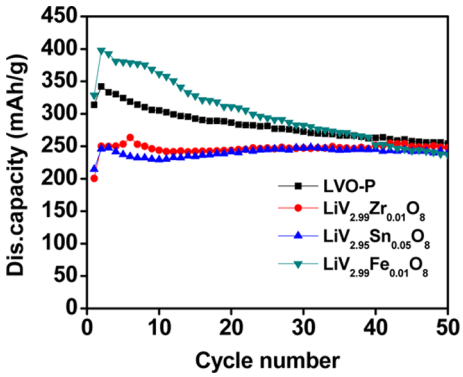

Figure 11. Cycling stability for the selected compounds LVO-P, $LiV_{2.99}Zr_{0.01}O_8$, $LiV_{2.95}Sn_{0.05}O_8$, and $LiV_{2.99}$ $Fe_{0.01}O_8$.

on the 0.15 M of molybdenum-doped LiV_3O_8 nanosheets with a surface area of 24.8 m^2/g to deliver a capacity of 217 and 206 mA h/g at the initial and 100th cycle, respectively, for a current density of 300 mA/g. The electrical conductivities of the bare and 0.15 M of molybdenum-doped LiV_3O_8 nanosheets were reported to be 3.52×10^{-6} and 2.89×10^{-5} S/cm, respectively. Nevertheless in our case, molybdenum doping was not found to improve the performance of LiV_3O_8, at any of the doping level.

Overall, as discussed under electrical studies, though the electrical conductivity of doped compounds were in the same order as that of LVO-P, the percentage of ionic and electronic conductivity values observed from transference number studies highly affected the electrochemical performance. The higher the percentage of ionic conductivity, the higher was the discharge capacity, as in the case of compound $LiV_{2.99}Fe_{0.01}O_8$. However, its lower percentage of electronic conductivity resulted in a poor cycling stability. The compounds, $LiV_{2.99}Zr_{0.01}O_8$ and $LiV_{2.95}Sn_{0.05}O_8$, with a good mixed conduction nature showed good cycling stability, as discussed above.

CONCLUSIONS

LiV_3O_8 was prepared via the most simple and cost-effective reflux method. The presence of polymer P123 in the preparation was found to affect the percentage of ionic and electronic conduction, which in turn influences the capacity and cycling stability of the cells, respectively. The effect of different levels of doping with different elements on the structure, electrical, and electrochemical performance of the compound was investigated. Among all doped compounds, $LiV_{2.99}Zr_{0.01}O_8$ and $LiV_{2.95}Sn_{0.05}O_8$ was found to deliver the best electrochemical performance both in terms of higher discharge capacity (∼250 mA h/g) and cycling stability (∼98%). The above compounds exhibited a mixed conducting nature with ∼60% of ionic and ∼40% of electronic conductivity. Though the compound $LiV_{2.99}Fe_{0.01}O_8$ was found to exhibit the best discharge capacity of 398 mA h/g for a current density of 30 mA/g because of its high percentage of ionic conductivity of ∼83%, its cycling stability was found to be degraded because of its poor percentage of electronic conductivity of ∼17%. We conclude that, the type and level of doping will successfully enhance the electrochemical properties of the parent compound only when it exhibits a mixed conducting nature.

EXPERIMENTAL SECTION

Pristine and doped lithium trivanadate compounds were prepared by the Pluronic P123-assisted reflux method. LVO-P: Initially 6 mM polymer (Pluronic P123, Aldrich) was dissolved in 100 mL of distilled water, and a homogenous viscous solution was obtained. To this, 0.1 M lithium acetate and 0.3 M ammonium metavanadate were added and refluxed for 2 h in a constant temperature oil bath at a temperature of 120 °C. The resultant solution was evaporated on a hot plate, and the dry residue was collected. The fine powder was then calcinated at 550 °C for about 10 h in air at a heating rate of 3 °C/min. A similar procedure was followed for all doped compounds. The raw materials for different doped $LiV_{3-x}M_xO_8$ (M = Zn, Co, Fe, Sn, Ti, Zr, Nb, and Mo) compounds were zinc acetate, cobalt acetate, iron citrate, tin chloride, titanium oxysulfate, zirconyl nitrate, niobium pentoxide, and molybdenum oxide, respectively. Doping was made at three different levels of x = 0.01/0.05/0.1 M. LVO-WP: For comparison, LiV_3O_8 was also prepared by refluxing the required amount of lithium acetate and ammonium metavanadate in the absence of the polymer P123, and the fine powder was calcinated in the same way as done for LVO-P.

Material Characterization. The structure of the pristine and doped compounds were examined by an X-ray diffractometer (Bruker D8) equipped with Cu Kα-radiation, and the lattice parameter values were obtained by TOPAS software version 4.2. The morphology of the compounds was analyzed by a scanning electron microscope (JEOL JSM-6700F). Raman spectrometer (model LabRAM HR Evolution, HORIBA Scientific) with a wavelength of 514 nm, and a power of 100 mW was used for the Raman studies.

For electrical studies, pellets with a diameter of 1 cm at a pressure of ten tons were made using hydraulic pellet press, and the pressed pellets were sandwiched between aluminum blocking electrodes and subjected to electrical studies. The ac impedance study was performed using a computer controlled

DOI: 10.1021/acsomega.7b01904
ACS Omega 2018, 3, 3036−3044

CH Instrument (CHI-600E) with a fixed amplitude voltage of 10 mV. Four-probe measurements made by SES Instruments (India) Pvt. Ltd were used to find the dc conductivity. The percentages of ionic and electronic conductivities of the compounds were found by transference number measurements carried out using a Keithley 4001 source meter.

For electrochemical testing, slurries were prepared by mixing the as-prepared active material (LVO), Super P carbon black, and poly(vinylidene fluoride) (Kynar 2801) binder (70:15:15 in wt %) dissolved in *N*-methyl pyrrolidone under stirring for 24 h. The electrodes were made by coating the slurry onto the Al foil. The composite electrodes were kept in a vacuum oven for 24 h at 70 °C. The CR2016 coin-type cells were assembled with the above cathodes, lithium metal as the anode (Kyokuto Metal Co., Japan), and Celgard 2502 film as the separator. A solution of 1 M $LiPF_6$ in ethylene carbonate and dimethyl carbonate (1:1, v/v) (Merck) was used as the electrolyte. The coin cells were assembled in an Ar-filled glovebox at an O_2 and H_2O level of less than 1 ppm. The cyclic voltammogram was made in the voltage range of 2−4 V (at a scan rate of 0.058 mV/S) using a MacPile II (BioLogic, France) system. Galvanostatic cycling was carried out at room temperature (25 °C) in the voltage range of 2−4 V at a current rate of 0.1 C by using Bitrode multiple battery testers (model SCN, Bitrode, USA).

■ ASSOCIATED CONTENT

Supporting Information

The Supporting Information is available free of charge on the ACS Publications website at DOI: 10.1021/acsomega.7b01904.

XRD patterns of $LiV_{2.99}M_{0.01}O_8$ and $LiV_{2.9}M_{0.1}O_8$ (M = Zn/Co/Fe/Sn/Ti/Zr/Nb/Mo) compounds, conductivity spectra of LVO-P, LVO-WP, $LiV_{2.99}Zr_{0.01}O_8$, $LiV_{2.95}Sn_{0.05}O_8$, and $LiV_{2.99}Fe_{0.01}O_8$ compounds, V/I spectra of LVO-P, LVO-WP, $LiV_{2.99}Zr_{0.01}O_8$, $LiV_{2.95}Sn_{0.05}O_8$, and $LiV_{2.99}Fe_{0.01}O_8$ compounds, and comparison of the interlayer distance (PDF)

■ AUTHOR INFORMATION

Corresponding Authors

*E-mail: meetsaku@gmail.com (Sakunthala Ayyasamy).

*E-mail: phymvvr@nus.edu.sg, msemvvr@nus.edu.sg, reddymvvr@gmail.com (M.V.R.).

ORCID

Stefan Adams: 0000-0003-0710-135X

M. V. Reddy: 0000-0002-6979-5345

Notes

The authors declare no competing financial interest.

■ ACKNOWLEDGMENTS

The authors would like to thank the Karunya University, Coimbatore-641114 for the central research facilities. The authors are grateful to the Science and Engineering Research Board (SERB), Department of Science and Technology, New Delhi, India, (DST Project no. SR/FTP/PS-192/2011) for providing funding for this research work. P.S.K. thanks the NUS-IRI for providing fellowship and research opportunities at the NUS. M.V.R. and S.A. thank the National Research Foundation (NRF), Prime Minister's Office, Singapore, for support under its Competitive Research Programme (CRP award NRF-CRP 10-2012-6).

■ REFERENCES

(1) Whittingham, M. S. Lithium Batteries and Cathode Materials. *Chem. Rev.* **2004**, *104*, 4271−4302.

(2) Armand, M.; Tarascon, J.-M. Building Better Batteries. *Nature* **2008**, *451*, 652−657.

(3) Goodenough, J. B.; Kim, Y. Challenges for Rechargeable Li Batteries. *Chem. Mater.* **2010**, *22*, 587−603.

(4) Chan, C. K.; Peng, H.; Liu, G.; McIlwrath, K.; Zhang, X. F.; Huggins, R. A.; Cui, Y. High Performance Lithium Battery Anodes Using Silicon Nanowires. *Nat. Nanotechnol.* **2008**, *3*, 31−35.

(5) Seong, I. W.; Hong, C. H.; Kim, B. K.; Yoon, W. Y. The Effects of Current Density and Amount of Discharge on Dendrite Formation in the Lithium Powder Anode Electrode. *J. Power Sources* **2008**, *178*, 769−773.

(6) Yamaki, J.-I.; Tobishima, S.-I.; Sakurai, Y.; Saito, K.-I.; Hayashi, K. Safety Evaluation of Rechargeable Cells with Lithium Metal Anodes and Amorphous V_2O_5 Cathodes. *J. Appl. Electrochem.* **1998**, *28*, 135−140.

(7) Lee, J. H.; Lee, J. K.; Yoon, W. Y. Electrochemical Analysis of the Effect of Cr Coating the LiV_3O_8 Cathode in a Lithium Ion Battery with a Lithium Powder Anode. *ACS Appl. Mater. Interfaces* **2013**, *5*, 7058−7064.

(8) Feng, Y.; Li, Y.; Hou, F. Preparation and Electrochemical Properties of Cr Doped LiV_3O_8 Cathode for Lithium Ion Batteries. *Mater. Lett.* **2009**, *63*, 1338−1340.

(9) Ren, X.; Hu, S.; Shi, C.; Zhang, P.; Yuan, Q.; Liu, J. Preparation and Electrochemical Properties of Zr Doped LiV_3O_8 Cathode Materials for Lithium Ion Batteries. *J. Solid State Electrochem.* **2012**, *16*, 2135−2141.

(10) Wadsley, A. D. Crystal Chemistry of Non-stoichiometric Pentavalent Vanadium Oxides: Crystal Structure of Li1+xV3O8. *Acta Crystallogr.* **1957**, *10*, 261−267.

(11) Pan, A.; Zhang, J.; Cao, G.; Liang, S.; Wang, C.; Nie, Z.; Jie, X.; Arey, B. W.; Xu, W.; Liu, D.; Xiao, J.; Li, G.; Liu, J. Nanosheet-structured LiV3O8 with High Capacity and Excellent Stability for High Energy Lithium Batteries. *J. Mater. Chem.* **2011**, *21*, 10077−10084.

(12) Zhang, H.-L.; Neilson, J. R.; Morse, D. E. Vapor-Diffusion-Controlled Sol−Gel Synthesis of Flaky Lithium Vanadium Oxide and Its Electrochemical Behavior. *J. Phys. Chem. C* **2010**, *114*, 19550−19555.

(13) Sakunthala, A.; Reddy, M. V.; Selvasekarapandian, S.; Chowdari, B. V. R.; Selvin, P. C. Preparation, Characterization, and Electrochemical Performance of Lithium Trivanadate Rods by a Surfactant-Assisted Polymer Precursor Method for Lithium Batteries. *J. Phys. Chem. C* **2010**, *114*, 8099−8107.

(14) Jiao, L.; Li, H.; Yuan, H.; Wang, Y. Preparation of Copper Doped LiV_3O_8 Composite by a Simple Addition of the Doping Metal as Cathode Materials for Lithium Ion Batteries. *Mater. Lett.* **2008**, *62*, 3937−3939.

(15) Pasquali, M.; Pistoia, G. Lithium Intercalation in $Na_{1+x}V_3O_8$ Synthesized by a Solution Technique. *Electrochim. Acta* **1991**, *36*, 1549−1553.

(16) Pistoia, G.; Wang, G.; Zane, D. Mixed Na/K Vanadates for Rechargeable Li batteries. *Solid State Ionics* **1995**, *76*, 285−290.

(17) Sun, J.; Jiao, L.; Yuan, H.; Liu, L.; Wei, X.; Miao, Y.; Yang, L.; Wang, Y. Preparation and Electrochemical Performance of $Ag_xLi_{1-x}V_3O_8$. *J. Alloys Compd.* **2009**, *472*, 363−366.

(18) Feng, C. Q.; Huang, L. F.; Guo, Z. P.; Wang, J. Z.; Liu, H. K. Synthesis and Electrochemical Properties of $LiY_{0.1}V_3O_8$. *J. Power Sources* **2007**, *174*, 548−551.

(19) Pouchko, S. V.; Ivanov-Schitz, A. K.; Kulova, T. L.; Skundin, A. M.; Turevskaya, E. P. Sol−gel Fabrication and Lithium Insertion Kinetics of the Mo-doped Lithium Vanadium Oxide Thin Films $Li_{1+x}Mo_yV_{3-y}O_8$. *Solid State Ionics* **2002**, *151*, 129−140.

(20) Zhao, M.; Jiao, L.; Yuan, H.; Feng, Y.; Zhang, M. Study on the Silicon Doped Lithium Trivanadate as Cathode Material for Rechargeable Lithium Batteries. *Solid State Ionics* **2007**, *178*, 387−391.

(21) Liu, L.; Jiao, L.; Sun, J.; Zhao, M.; Zhang, Y.; Yuan, H.; Wang, Y. Electrochemical Performance of $LiV_{3-2x}Ni_xMn_xO_8$ Cathode Materials

DOI: 10.1021/acsomega.7b01904
ACS Omega 2018, 3, 3036−3044

Synthesized by the Sol−gel Method. *Solid State Ionics* **2008**, *178*, 1756−1761.
(22) Liu, L.; Jiao, L.; Sun, J.; Zhang, Y.; Zhao, M.; Yuan, H.; Wang, Y. Electrochemical Performance of $LiV_{3-x}Ni_xO_8$ Cathode Materials Synthesized by a Novel Low Temperature Solid State Method. *Electrochim. Acta* **2008**, *53*, 7321−7325.
(23) Senthil Kumar, P.; Sakunthala, A.; Prabu, M.; Reddy, M. V.; Joshi, R. Structure and Electrical Properties of Lithium Nickel Manganese Oxide (LiNi0.5Mn0.5O2) Prepared by P123 Assisted Hydrothermal Route. *Solid State Ionics* **2014**, *267*, 1−8.
(24) Senthil Kumar, P.; Sakunthala, A.; Reddy, M. V.; Shanmugam, S.; Prabu, M. Correlation Between the Structural, Electrical and Electrochemical Performance of Layered $Li(Ni_{0.33}Co_{0.33}Mn_{0.33})O_2$ for Lithium Ion Battery. *J. Solid State Electrochem.* **2016**, *20*, 1865−1876.
(25) Kawakita, J.; Kato, T.; Katayama, Y.; Miura, T.; Kishi, T. Lithium Insertion Behaviour of $Li_{1+x}V_3O_8$ with Different Degrees of Crystallinity. *J. Power Sources* **1999**, *81*−*82*, 448−453.
(26) Liu, G. Q.; Zeng, C. L.; Yang, K. Study on the Synthesis and Properties of LiV_3O_8 Rechargeable Lithium Batteries Cathode. *Electrochim. Acta* **2002**, *47*, 3239−3243.
(27) Liu, L.; Jiao, L.; Sun, J.; Zhang, Y.; Zhao, M.; Yuan, H.; Wang, Y. Electrochemical Properties of Submicron Sized LiV_3O_8 Synthesized by a Low Temperature Reaction Route. *J. Alloys Compd.* **2009**, *471*, 352−356.
(28) Feng, Y.; Hou, F.; Li, Y. A New Low Temperature Synthesis and Electrochemical Properties of $LiV3O_8$ Hydrate as Cathode Material for Lithium Ion Batteries. *J. Power Sources* **2009**, *192*, 708−713.
(29) Xu, H. Y.; Wang, H.; Song, Z. Q.; Wang, Y. W.; Yan, H.; Yoshimura, M. Novel Chemical Method for Synthesis of LiV_3O_8 Nanorods as Cathode Materials for Lithium Ion Batteries. *Electrochim. Acta* **2004**, *49*, 349−353.
(30) Liu, H.; Yang, H.; Huang, T. Synthesis, Structure and Electrochemical Properties of One Dimensional Nanometer Materials LiV_3O_8. *Mater. Sci. Eng., B* **2007**, *143*, 60−63.
(31) Yang, G.; Wang, G.; Hou, W. Microwave Solid State Synthesis of LiV_3O_8 as Cathode Material for Lithium Batteries. *J. Phys. Chem. B* **2005**, *109*, 11186−11196.
(32) Zhang, X.; Frech, R. Spectroscopic Investigation of $Li_{1+x}V_3O_8$. *Electrochim. Acta* **1998**, *43*, 861−868.
(33) Reddy, M. V.; Subba Rao, G. V.; Chowdari, B. V. R. Cathodic behaviour of NiO-coated $Li(Ni_{1/2}Mn_{1/2})O_2$. *Electrochim. Acta* **2005**, *50* (16-17), 3375−3382.
(34) Tey, S. L.; Reddy, M. V.; Subba Rao, G. V.; Chowdari, B. V. R.; Yi, J. B.; Ding, J.; Vittal, J. J. Synthesis, structure, and magnetic properties of $[Li(H_2O)M(N_2H_3CO_2)_3]\cdot 0.5H_2O$ (M = Co,Ni) as single precursors to $LiMO_2$ battery materials. *Chem. Mater.* **2006**, *18* (6), 1587−1594.
(35) Saravanan, K.; Vittal, J. J.; Reddy, M. V.; Chowdari, B. V. R.; Balaya, P. Storage performance of $LiFe_{1-x}Mn_xPO_4$ nanoplates (x = 0, 0.5, and 1). *J. Solid State Electrochem.* **2010**, *14* (10), 1755−1760.
(36) Xu, X.; Luo, Y.-Z.; Mai, L.-Q.; Zhao, Y.-L.; An, Q.-Y.; Xu, L.; Hu, F.; Zhang, L.; Zhang, Q.-J. Topotactically Synthesized Ultralong LiV_3O_8 Nanowire Cathode Materials for High-rate and Long-life Rechargeable Lithium Batteries. *NPG Asia Mater.* **2012**, *4*, No. e20.
(37) Kawakita, J.; Katayama, Y.; Miura, T.; Kishi, T. Structural Properties of $Li_{1+x}V_3O_8$ Upon Lithium Insertion at Ambient and High Temperature. *Solid State Ionics* **1998**, *107*, 145−152.
(38) Kawakita, J.; Miura, Y.; Kishi, T. Lithium Insertion and Extraction Kinetics of $Li1_{+x}V_3O_8$. *J. Power Sources* **1999**, *83*, 79−83.
(39) Song, H.; Liu, Y.; Zhang, C.; Liu, C.; Cao, G. Mo-doped LiV_3O_8 Nanorod Assembled Nanosheets as a High Performance Cathode Material for Lithium Ion Batteries. *J. Mater. Chem. A* **2015**, *3*, 3547−3558.
(40) Kawakita, J.; Majima, M.; Miura, T.; Kishi, T. Preparation and Lithium Insertion Behaviour of Oxygen Deficient $Li_{1+x}V_3O_{8-\delta}$. *J. Power Sources* **1997**, *66*, 135−139.
(41) Caes, S.; Arrebola, J. C.; Krins, N.; Eloy, P.; Gaigneaux, E. M.; Henrist, C.; Cloots, R.; Vertruyen, B. Mesoporous Lithium Vanadium Oxide as a Thin Film Electrode for Lithium-Ion Batteries: Comparison Between Direct Synthesis of LiV_2O_5 and Electrochemical Lithium Intercalation in V_2O_5. *J. Mater. Chem. A* **2014**, *2*, 5809−5815.
(42) Huang, S.; Tu, J. P.; Jian, X. M.; Lu, Y.; Shi, S. J.; Zhao, X. Y.; Wang, T. Q.; Wang, X. L.; Gu, C. D. Enhanced Electrochemical Properties of Al_2O_3-coated LiV_3O_8 Cathode Materials for High-Power Lithium-Ion Batteries. *J. Power Sources* **2014**, *245*, 698−705.

DOI: 10.1021/acsomega.7b01904
ACS Omega 2018, 3, 3036−3044